Wave Motion 89 (2019) 57–64

Contents lists available at ScienceDirect

Wave Motion

journal homepage: www.elsevier.com/locate/wamot

A modified Hankinson Equation for the wave speed of laser ultrasound in Radiata Pine

Kasper van Wijk *, Jonathan Simpson, Sam Hitchman

Dodd-Walls Centre for Photonic and Quantum Technologies and The Physical Acoustics Lab, Department of Physics, University of Auckland, New Zealand

HIGHLIGHTS

- We introduce a Laser-based, non-contacting, and non-destructive system for ultrasound in wood.
- Scanning ultrasonic waves reveal the orthotropic properties of wood, with the fast direction parallel to the grain.
- The observed angular dependence of ultrasonic speed is well-described by a Modified Hankinson Equation.
- Details of laser ultrasound provide information about the heterogeneity of wood, such as knots or pith.

ARTICLE INFO

Article history:
Received 12 September 2018
Received in revised form 8 January 2019
Accepted 6 March 2019
Available online 12 March 2019

ABSTRACT

The physical properties of wood are of interest in a wide range of applications, including biology, climate science, and civil engineering. Its orthotropic nature poses considerable challenges in assessing the fully three-dimensional properties of wood. Laser ultrasonic waveforms of Radiata Pine of differing quality illustrate opportunities to extract its angle-dependent physical properties. We present a newly-derived Modified Hankinson Equation that improves the fit to the observed angle-dependence of wave speed in the higher quality sample by almost a factor of 3 to the original Hankinson Equation. Wave forms in the lower quality sample detect small-scale heterogeneity (due to pith, in this case), based on variations in ultrasonic wave speed and attenuation.

© 2019 Elsevier B.V. All rights reserved.

1. Introduction

The physical properties of wood are orthotropic with a cylindrical symmetry, because of the combination of a predominantly vertical grain structure and horizontal annual growth rings. Bending tests are the gold standard to test the strength of timber for the construction industry, but ultrasonic techniques provide some significant advantages. Elastic wave velocities are sensitive to differences in timber species, moisture content, temperature, and direction of propagation [1]. The probing wavelengths of ultrasound are short, so that the resolution is higher than the information a bending test of an entire timber board provides. Bucur and Archer [2] showed that the elastic constants of wood can be estimated from the velocity of elastic waves and the density, while Sandoz [3] used ultrasonic wave speeds to sort beams of spruce into three classes. In both cases contacting piezoelectric transducers were used to measure the first arrival (the primary or P-wave) speed parallel to the grain.

Exciting and detecting elastic waves in wood from stand-off distances avoids the mechanical ringing and coupling issues associated with ultrasonic transducers. Air-coupled speakers and microphones form an alternative, but the strong

* Corresponding author.
E-mail address: k.vanwijk@auckland.ac.nz (K. van Wijk).

https://doi.org/10.1016/j.wavemoti.2019.03.005
0165-2125/© 2019 Elsevier B.V. All rights reserved.

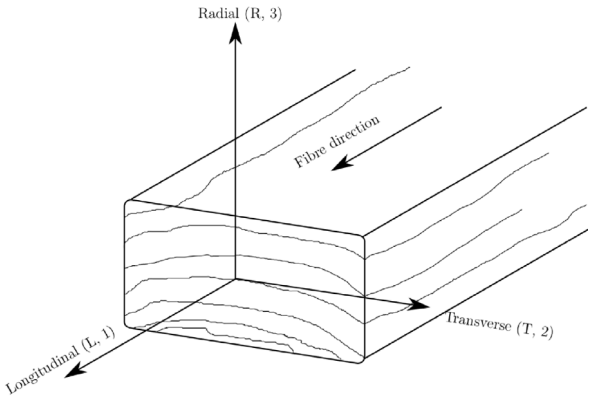

Fig. 1. The principal axes of wood with respect to the grain direction and growth rings in a typical wood sample used for construction. We define the Longitudinal (grain) direction as axis 1, Transverse as axis 2, and Radial as axis 3.

acoustic impedance contrast between air and wood results in large coupling losses. Still, air-coupled ultrasonic transducers have been successfully used to estimate the quality of glued wooden planks [4] and wooden beams [5]. More recently, light has been used to identify wood fibre orientation [6], and decay in historic wooden buildings [7]. But light can also excite elastic waves via the photoacoustic effect, first observed by Bell [8]. This way, light has advantages over transducer measurements, as no physical contact is required. Combined with a Laser Doppler Vibrometer as a detector of ultrasound, applications of laser-based ultrasonics have recently led to successful applications in rocks [9], apples [10,11], ice [12], and human tissue [13], for example.

Kuo et al. [14] used laser light with a modulated intensity to excite sound waves, which are detected using a non-contacting microphone, in small samples of wood. As the amplitude of excited sound waves is proportional to the wavelength of the light, the infra-red (IR) absorption spectrum of wood was determined. Based on the IR spectrum presented by Kuo et al. [14], and non-contacting optical detectors outlined by Scruby and Drain [15], Bucur [16] theorized that traditional transducer measurements could be reproduced using a full laser-based non-contacting ultrasonics set-up.

Here, we derive a novel modification to the Hankinson Equation: a popular equation sometimes invoked to explain the angular dependence of ultrasonic wave speed in timber [e.g., 17–20]. Second, we present the first fully non-contacting laser ultrasonic measurements on timber, introducing the hardware and the geometry of the acquisition system. Finally, ultrasonic wave fields in two samples of Radiata Pine illustrate that this non-contacting setup is: (1) well-suited to record spatially dense data to study heterogeneity in timber, and (2) shows that in relatively homogeneous timber the Modified Hankinson Equation improves the fit to the data by a factor of almost 3, compared to the original Hankinson Equation.

2. Theory

The bulk physical properties of wood follow a cylindrical symmetry. They vary longitudinally with the grain, and radially and transversely from annual rings. From here on, we denote these axes of symmetry as L or 1, T or 2, and R or 3, respectively (Fig. 1). Typically, timber is cut to closely – but not perfectly – follow the grain direction (L,1). Existing measurements [21] indicate that in many wood types the difference between the radial and transverse properties are small compared to those on the longitudinal (grain) direction, which means wood can be approximated as transversely isotropic. Several empirical models have been developed to determine the angular dependence of the physical properties of wood. Hankinson [22] developed a formula – following the notation of Bodig and Jayne [23] – where the property N depends on the angle θ with the grain as

$$N(\theta) = \frac{PQ}{P\sin^2\theta + Q\cos^2\theta}. \tag{1}$$

P is the property parallel to the grain, and Q is the property perpendicular to the grain. In Hankinson [22], this property was the uniaxial compressive strength. Lang et al. [24] showed the Hankinson Equation (HE) can be extended to the Young's modulus E, a measure of the stiffness of a solid material:

$$E(\theta) = \frac{E_L E_T}{E_L\sin^2\theta + E_T\cos^2\theta} \tag{2}$$

where subscripts L and T indicate the Longitudinal and Transverse directions, respectively.

After the original application to (static) physical properties of wood, the HE was used for the dynamic ultrasonic velocity V by substitution of $N = V$ [e.g., 17–20]:

$$V(\theta) = \frac{V_L V_T}{V_L\sin^2\theta + V_T\cos^2\theta}. \tag{3}$$

However, we propose a modified HE based on $N = V^2$. For wave propagation in one dimension, there is a straightforward relationship between the Young's modulus and the P-wave speed V:

$$V^2 = \frac{E}{\rho}, \tag{4}$$

where ρ is the density. In higher dimensions, however, compression and dilation caused by the wave results in deformation in the direction(s) orthogonal to propagation. The Poisson's ratio ν expresses the ratio between the strain in transverse and axial directions. Based on Mah and Schmitt [25] and Murray [21], the P-wave speed of wood parallel to the grain (Longitudinal, 1) in 3D is:

$$V_1^2 = \frac{E_{11}\,(1 - \nu_{32}\nu_{23})}{\rho\Delta}, \tag{5}$$

where $E_{11} = E_L$, $\Delta = (1 - \nu_{12}\nu_{21} - \nu_{23}\nu_{32} - \nu_{31}\nu_{13} - 2\nu_{21}\nu_{32}\nu_{13})$ and ν_{ij} is the Poisson's ratio that describes the change of shape in direction j for a deformation in i. In the transverse and radial directions,

$$V_2^2 = \frac{E_{22}\,(1 - \nu_{31}\nu_{13})}{\rho\Delta}, \tag{6}$$

$$V_3^2 = \frac{E_{33}\,(1 - \nu_{21}\nu_{12})}{\rho\Delta}, \tag{7}$$

where $E_{22} = E_T$ and $E_{33} = E_R$.

Combining Eqs. (5), (6) and (2) results in the following Modified Hankinson Equation (MHE):

$$V(\theta) \approx \frac{V_L V_T}{\sqrt{V_L^2 \sin^2\theta + V_T^2 \cos^2\theta}}, \tag{8}$$

where the dependence on density ρ and Δ is negated by taking the ratio of the square of the wave speeds in orthogonal directions. Eq. (8) assumes small values of the (squared) Poisson's ratios [e.g., Table 4.2 in 1], or that

$$\nu_{32}\nu_{23} \approx \nu_{31}\nu_{13}. \tag{9}$$

Expression (8) presents a different angular dependence on V than Eq. (3), through differences in the denominator.

3. Methods

We investigate the physical properties of New Zealand Radiata Pine, pictured in Fig. 2. These samples are labelled SG6 (top) and SG12 (bottom), respectively. The letters stand for "Structural Grade", whereas the numerical value is an estimate of the longitudinal Young's Modulus E_L in units of GPa. This estimate is based on a bending test. Our samples are small pieces taken from 3 m long boards. Quality assessment (visual and bending tests) is done on the entire board, so that local variations in quality cannot be ruled out. The average densities of our samples are measured at 567 kg/m^3 for the SG12, and 336 kg/m^3 for the SG6 sample. The dimensions of the SG6 sample are 45 × 90 × 374 mm, and the SG12 sample measures 43 × 88 × 295 mm.

Fig. 3 is an annotated photograph of the experimental set-up. A short high-powered laser pulse (Radiant from OPOTEK, the wavelength is 680 nm, focused to a spot size of 1 mm diameter) induces ultrasonic waves into our sample, recorded at the centre of a circle of radius 34 mm with a Laser Doppler Vibrometer (Polytec OFV505 LDV head, with the OFV5000 controller, and the VD09 decoder card). The laser source energy of 32 mJ per pulse results in superficial burn spots in the sample, and ablated purple dye on sample SG12. The receiver spot size is less than 1 mm in diameter. Signal strength is maximized by applying a small piece of reflective tape to the wood. Each waveform is amplified by a factor of 5 in an SRS560 pre-amplifier, and is the average of 300 realizations. The wood sample is placed on a rotational stage (Newport URS100BCC), recording a wave field every two degrees of rotation. The entire data acquisition is automated with the Python-based PLACE package [26]. Each scan takes 60 min to complete, dominated by the limitation of the source laser operating at the maximum repetition rate of 20 Hz. All data presented here are available [27].

4. Results

Fig. 4 presents wave fields as a function of angle with the longitudinal direction, for SG12. These waveforms are normalized to the largest recorded amplitude in the scan. One of the coherent arrivals across all angles is the first-arriving event, called the primary wave (P-wave, for short). The fast P-wave directions are 0 and 180 degrees, with the slow direction at 90 and 270 degrees, relative to the grain of the sample (longitudinal direction). The dominant frequency of this arrival varies between 200 kHz (slow direction) and 500 kHz (fast direction). This pattern is repeated later in time for a surface wave arrival. In the time between these waves, a P-wave arrives that is reflected off the side of the wood closest to 90 and 270 degrees.

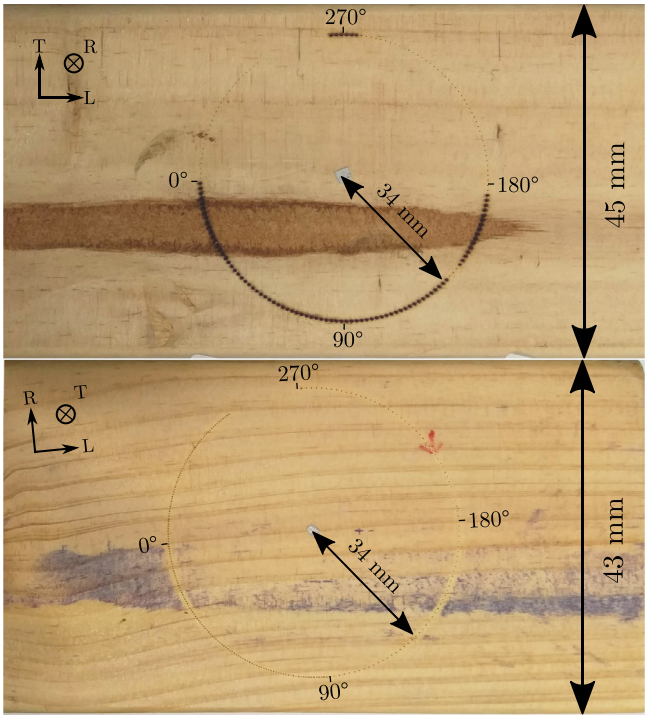

Fig. 2. Timber samples SG6 (top) and SG12 (bottom), showing the locations of the circular scans on the face of the boards, and the radial (R), longitudinal (L), and transverse (T) axes.

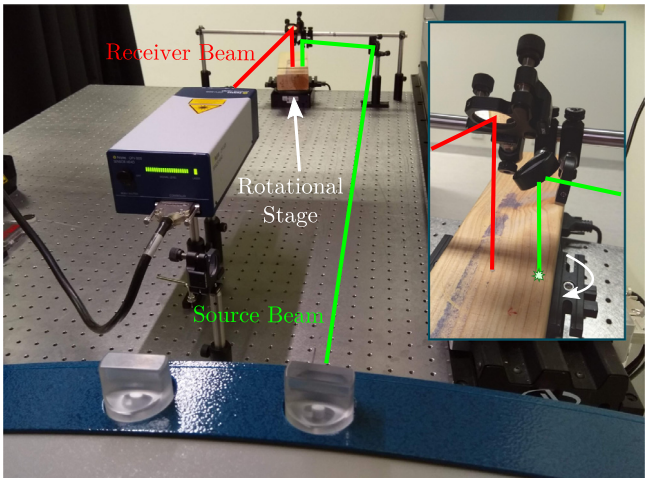

Fig. 3. Experimental setup to acquire laser ultrasound as a function of angle in samples of Radiata Pine. The inset provides a close-up view of the source and receiver laser beam locations on the wood.

The identical experiment performed in SG6 (Fig. 5) shows some of the same coherent waves arriving, but the variations in arrival time and wave amplitude with angle are more complicated. Similar to SG12, the fast direction is close to the longitudinal axis for sample SG6 (−10, and 180 degrees), but the slowest direction is around 30 degrees to the grain, for both the P- and the surface wave. The dominant frequency of this arrival varies between 200 kHz (slow) and 300 kHz (fast). Overall, wave amplitudes are lower than in SG12. This means, for example, that the reflection of the P-wave from the sides of the sample is not visible. The energy in the waveforms, as well as the arrival time variations, are more heterogeneous in SG6 than in SG12. Particularly, the 10–40 and 140–170 degree ranges show anomalously large energy, compared to the rest of the waveforms in this scan. In addition, the P-wave arrival time in SG6 does not decrease as smoothly from 10 to 40 degrees, as in SG12.

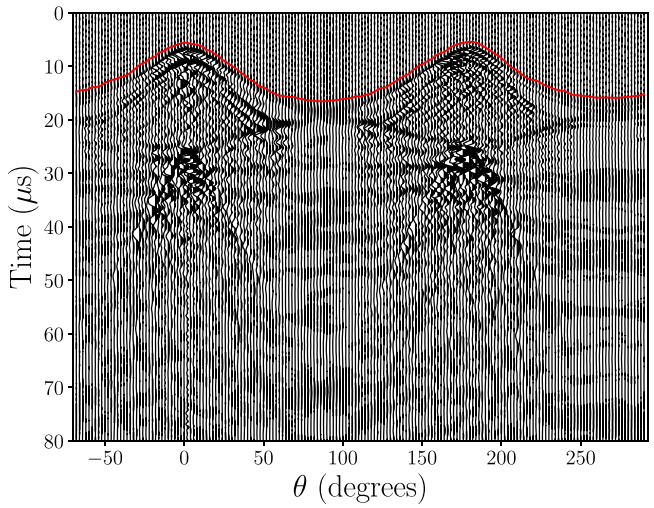

Fig. 4. Ultrasonic wave fields as a function of angle for sample SG12. The red line indicates the first arrival of ultrasonic wave energy.

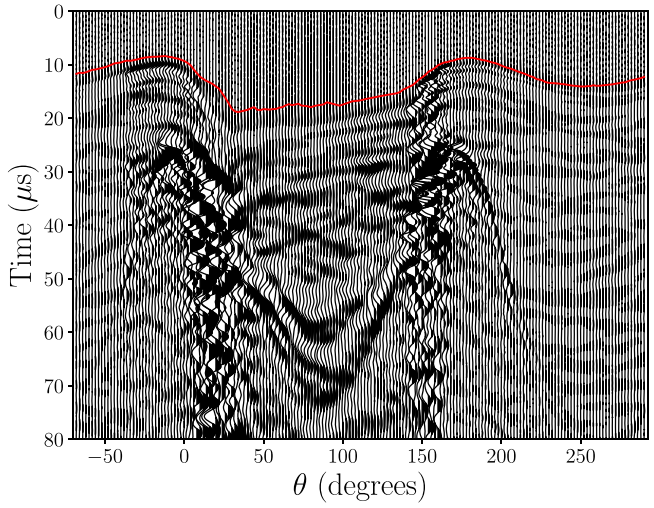

Fig. 5. Ultrasonic wave fields as a function of angle with the grain for SG6. The red line indicates the arrival time of the primary wave.

Software based on Dynamic Time Warping automatically estimates the P-wave arrival times [28] by picking the first break of the primary wave. For positions where the Dynamic Time Warping pick deviated slightly from the first break, the P-wave was manually picked (less than 10 positions per scan). The P-wave arrivals are converted to P-wave speeds and plotted as a function of angle for both samples in Fig. 6. Because the source and receiver spot sizes are much smaller than the dominant wavelengths, this represents the group wave speed, rather than the phase speed [29]. We estimate the (average) standard deviation of the speed to be 0.10 km/s, based on a picking accuracy of 0.1 μs and a source–receiver distance estimate only accurate to 0.5 mm. The slow direction for the two samples is similar in speed, but the SG12 has a faster P-wave speed than SG6 in the longitudinal direction. In fact, for SG12 the ratio of fast to slow P-wave speed is 3, while for the SG6 it is 2. The fast and slow direction of surface waves in both samples match the orientation of the variations in P-wave speed. Interestingly, the surface waves are comparable in speed for both samples. This rose diagram also confirms the difference in heterogeneity of these samples, because the ellipsoid for SG12 is more uniform than the equivalent ellipsoid for SG6.

Fig. 7 compares the Hankinson Equation (HE) and the MHE to estimates of $V(\theta)$ in SG12. The root-mean-square (RMS) misfit to the data for the HE model is 0.39 km/s, whereas for the MHE model this is 0.14 km/s, an improvement of almost a factor of 3.

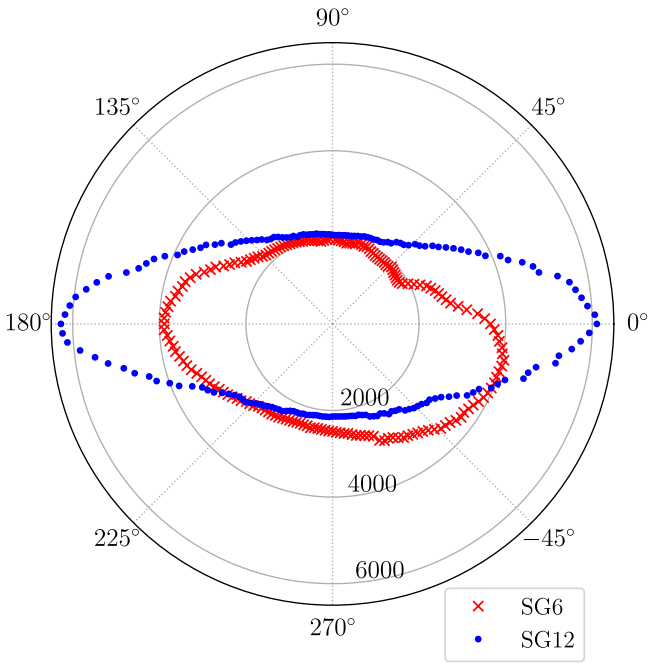

Fig. 6. A rose diagram of the P-wave speed in samples SG6 and SG12. The radial axis is the wave speed in m/s.

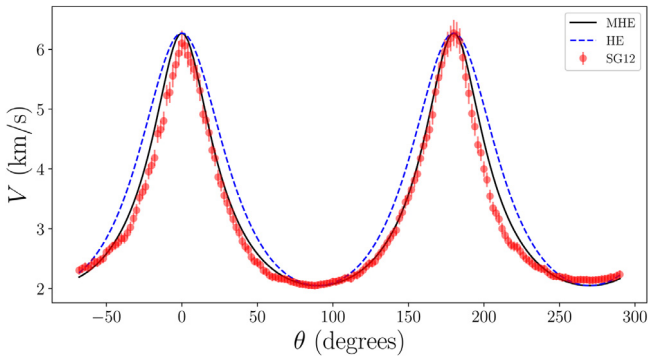

Fig. 7. The group velocity of the primary ultrasonic wave as a function of the angle with the grain, compared to (1) the prediction by the Hankinson equation (HE), and (2) the Modified Hankinson Equation (MHE).

5. Discussion

The group P-wave speed in the longitudinal directions is ∼6200 m/s and ∼4000 m/s for SG12 and SG6, respectively. If we assume the wave propagation is effectively 1D in this geometry, according to Eq. (4), $E_L \approx 6200^2 * 567 \approx 22$ GPa for SG12. This value is considerably higher than the estimate of the full 3 m board of 12 GPa. We offer four explanations for the discrepancy. First, it could be that our sample of SG12 is not representative of the 3 m long board. Second, Eq. (5) shows that Poisson's ratio plays a role. Unknown, but non-zero values, for Poisson's ratio can account for (part) of the over-estimation of E_L in 1D. Third, it is well known that static E is less than the dynamic E from wave propagation [20,30]. Finally, SG12 is the highest grade offered by this particular woodmill, which means a structural grade of 12 GPa indicates the *minimum* value of the bending test.

SG12 propagates higher frequency P-waves than SG6. Within each sample, the P-waves in the fast directions have higher frequency content than the P-wave in the slow directions. This connection between attenuation and wave speed described by Kramers–Kronig relationships is observed in many other applications. Rotational scans in anisotropic mudrocks with aligned clay platelets also make both wave speed and attenuation anisotropic [29]. The connection between water content and attenuation is well documented in many materials, but in this case the wood samples were (air) dry. Future work may involve relating the attenuative wave properties to moisture content for a range of applications in wood characterization.

We observe two examples of strong heterogeneity in SG6. First, waveforms recorded from 10–40 and 140–170 degrees display above average wave energy. These particular wave fields are generated on a darker area indicating pith, the softer core part of the tree (Fig. 2). On the darker pith, the absorption of the source laser light is more efficient than on the lighter coloured wood. Second, the arrival time of the P-wave from 0–180 degrees is greater and less regular than for 180–360 degrees, where the waves do not interact with the pith. This fully non-contacting laser ultrasound system showing the effects of pith on ultrasonic wave excitation and propagation allows us to pursue the detailed physical properties of wood. In future applications, automated scanning with short wavelengths for local variations may identify borings of insects [31], or provide detailed information about pith or knots in the wood [32].

The wave fields in SG12 are more consistent than in SG6, indicating a more homogeneous sample, suited to investigate the performance of the MHE, versus the HE. Both the fit to the data, as well as the theoretical arguments, suggest the MHE is a better representation of $V(\theta)$ than HE. Other studies of V using HE resort to adjusting the power on V between 1.5 and 2.5 to better the data fit [17–20]. However, the MHE does not require such an ad-hoc adjustment to fit $V(\theta)$ for SG12 on average within two standard deviations.

6. Conclusions

A new scanning laser ultrasonic system probes the physical properties of timber, as a function of angle with the grain direction. The resulting wave fields provide detailed information about the primary wave speed and attenuation of ultrasound, which vary strongly with angle in two samples of Radiata Pine. A newly derived Modified Hankinson Equation improves the fit to the observed angular dependence of the primary group wave speed in a higher-grade, more homogeneous sample by almost a factor of 3. High-resolution wave propagation and attenuation in a lower-grade sample provide detailed information about the presence of heterogeneity, in this case caused by the presence of pith.

Acknowledgements

We thank the University of Auckland, New Zealand and the Dodd-Walls Centre, New Zealand for their financial support of this research. We also acknowledge the support of Paul Freeman in the development of PLACE.

References

[1] D.W. Green, J.E. Winandy, D.E. Kretschmann, Mechanical properties of wood, Wood handbook: wood as an engineering material, in: General Technical Report FPL; GTR-113, Vol. 113, USDA Forest Service, Forest Products Laboratory, Madison, WI, 1999, pp. 4.1–4.45.
[2] V. Bucur, R.R. Archer, Elastic constants for wood by an ultrasonic method, Wood Sci. Technol. 18 (1984) 255–265, http://dx.doi.org/10.1007/BF00353361.
[3] J.L. Sandoz, Grading of construction timeber by ultrasound, Wood Sci. Technol. 23 (1989) 95–108, http://dx.doi.org/10.1007/BF00350611.
[4] S.J. Sanabria, C. Mueller, J. Neuenschwander, P. Niemz, U. Sennhauser, Air-coupled ultrasound as an accurate and reproducible method for bonding assessment of glued timber, Wood Sci. Technol. 45 (2011) 645–659, http://dx.doi.org/10.1007/s00226-010-0357-z.
[5] A. Kandemir-Yucel, A. Tavukcuoglu, E. Caner-Saltik, In situ assessment of structural timber elements of a historic building by infrared thermography and ultrasonic velocity, Infrared Phys. & Technol. 49 (2007) 243–248, http://dx.doi.org/10.1016/j.infrared.2006.06.012.
[6] S. Nieminen, J. Heikkinen, J. Rty, Laser transillumination imaging for determining wood defects and grain angle, Meas. Sci. Technol. 24 (2013) 125401.
[7] U. Dackermann, K. Crews, B. Kasal, J. Li, M. Riggio, F. Rinn, T. Tannert, In situ assessment of structural timber using stress-wave measurements, Mater. Struct. 47 (2014) 787–803, http://dx.doi.org/10.1617/s11527-013-0095-4.
[8] A.G. Bell, Art. xxxiv.–on the production and reproduction of sound by light, Am. J. Sci. (1880-1910) 20 (1880) 305.
[9] J.A. Scales, A.E. Malcolm, Laser characterization of ultrasonic wave propagation in random media, Phys. Rev. E 67 (2003) 046618.
[10] S. Hitchman, K. van Wijk, Z. Davidson, Monitoring attenuation and the elastic properties of an apple with laser ultrasound, Postharvest Biol. Technol. 121 (2016) 71–77.
[11] K. van Wijk, S. Hitchman, Apple seismology, Phys. Today 70 (2017) 94–95, http://dx.doi.org/10.1063/PT.3.3740, arXiv:http://dx.doi.org/10.1063/PT.3.3740.
[12] T.D. Mikesell, K. van Wijk, L.T. Otheim, H.-P. Marshall, A. Kurbatov, Laser ultrasound observations of mechanical property variations in ice cores, Geosciences 7 (2017) http://dx.doi.org/10.3390/geosciences7030047, URL: http://www.mdpi.com/2076-3263/7/3/47.
[13] J.L. Johnson, M. Merrilees, J. Shragge, K. van Wijk, All-optical extravascular laser-ultrasound and photoacoustic imaging of calcified atherosclerotic plaque in excised carotid artery, Photoacoustics 9 (2018) 62–72, http://dx.doi.org/10.1016/j.pacs.2018.01.002.
[14] M.-l. Kuo, J.F. McClelland, S. Luo, P.-L. Chien, R. Walker, C.-Y. Hse, Applications of infrared photoacoustic spectroscopy for wood samples, Wood Fiber Sci. 20 (1987) 132–145.
[15] C.B. Scruby, L.E. Drain, Laser Ultrasonics: Techniques and Applications, Adam Hilger, 1990.
[16] V. Bucur, Acoustics of Wood, Springer Science & Business Media, 2006.
[17] J.P. Armstrong, D.W. Patterson, J.E. Sneckenberger, Comparison of three equations for predicting stress wave velocity as a function of grain angle, Wood Fiber Sci. 23 (1991) 32–43.
[18] H. Xu, G. Xu, L. Wang, L. Yu, Propagation behavior of acoustic wave in wood, J. For. Res. 25 (2014) 671–676.
[19] R.M. Elsener, Material Characterization of Timber Utility Poles Using Experimental Approaches (Master's thesis), University of Technology Sydney, 2014.
[20] U. Dackermann, R. Elsener, J. Li, K. Crews, A comparative study of using static and ultrasonic material testing methods to determine the anisotropic material properties of wood, Constr. Build. Mater. 102 (2016) 963–976.
[21] Y.D. Murray, Manual for LS-DYNA Wood Material Model, Vol. 143, 2007.
[22] R.L. Hankinson, Investigation of crushing strength of spruce at varying angles of grain, Air Serv. Inf. Circ. 3 (1921) 130.
[23] J. Bodig, B.A. Jayne, Mechanics of Wood and Wood Composites, Van Nostrand Reinhold Company, New York, 1982.

[24] E.M. Lang, L. Bejo, F. Divos, Z. Kovacs, R.B. Anderson, Orthotropic strength and elasticity of hardwoods in relation to composite manufacture part iii: orthotropic elasticity of structural veneers, Wood Fiber Sci. 35 (2007) 308–320.
[25] M. Mah, D.R. Schmitt, Determination of the complete elastic stiffnesses from ultrasonic phase velocity measurements, J. Geophys. Res. 108 (2003) ECV 6–1–ECV 6–11, http://dx.doi.org/10.1029/2001JB001586, URL: https://agupubs.onlinelibrary.wiley.com/doi/abs/10.1029/2001JB001586.
[26] J.L. Johnson, H. tom Wörden, K. van Wijk, PLACE An open-source python package for laboratory automation, control, and experimentation, J. Lab. Autom. 20 (2015) 10–16.
[27] J. Simpson, K. van Wijk, S. Hitchman, Rotational Scans on Wood, 2018, http://dx.doi.org/10.17608/k6.auckland.7034063.v1, URL: https://figshare.com/articles/Rotational{_}scans{_}on{_}Wood/7034063.
[28] E.L. Durán, L. Adam, I.C. Wallis, A robust methodology for time-picking and error analysis of ultrasonic waveforms and rock densities in the laboratory, GEOPHYSICS (2019) 1–49, http://dx.doi.org/10.1190/geo2018-0331.1, arXiv:https://doi.org/10.1190/geo2018-0331.1.
[29] T.E. Blum, L. Adam, K. van Wijk, Noncontacting benchtop measurements of the elastic properties of shales, GEOPHYSICS 78 (2013) C25–C31, http://dx.doi.org/10.1190/geo2012-0314.1, URL: http://library.seg.org/doi/abs/101190/geo2012-03141.
[30] D. Ouis, On the frequency dependence of the modulus of elasticity of wood, Wood Sci. Technol. 36 (2002) 335–346.
[31] M. Zorović, A. Čokl, Laser vibrometry as a diagnostic tool for detecting wood-boring beetle larvae, J. Pest Sci. 88 (2015) 107–112, http://dx.doi.org/10.1007/s10340-014-0567-5.
[32] J.T. Karsulovic, L.A. León, L. Gaete, Ultrasonic detection of knots and annual ring orientation in pinus radiata lumber, Wood Fiber Sci. 32 (2007) 278–286.